



# 1 Correlation between tectonic stress regimes and methane seepage on 2 the west-Svalbard margin 3

4 Andrea Plaza-Faverola<sup>1</sup> and Marie Keiding<sup>2</sup>

5 <sup>1</sup> CAGE-Centre for Arctic Gas Hydrate, Environment, and Climate; Department of Geosciences, UiT The Arctic  
6 University of Norway, N-9037 Tromsø, Norway

7 <sup>2</sup> Geological Survey of Norway (NGU), P.O. Box 6315 Torgarden, 7491 Trondheim, Norway

8 *Correspondence to:* Andrea Plaza-Faverola (Andrea.a.faverola@uit.no)

9 **Abstract.** Methane seepage occurs across the west-Svalbard margin at water depths ranging from the upper shelf  
10 at < 300 m to gas hydrate systems in the deep sea at > 1000 m. The Vestnesa sedimentary ridge, located on oceanic  
11 crust between 1000-1700 m water depth, hosts a perennially stable gas hydrate system with evidence of both past  
12 and present-day seepage. On the ridge, an eastward transition from a zone with clear morphological evidence of  
13 past seepage to a zone of active present-day seepage coincides with a change in the faulting pattern of near-surface  
14 strata. We modelled the tectonic stress regime due to oblique spreading along the Molloy and Knipovich spreading  
15 ridges to investigate whether spatial and temporal variations in the regional stress field may explain patterns of  
16 seepage distribution. The model reveals a zone of tensile stress that extends northward from the Knipovich Ridge  
17 and encompasses a zone of active seepage and extensional faulting. A zone of past seepage is presently located in  
18 a strike-slip regime. Our modelling results suggest that seepage is promoted by opening of faults and fractures in  
19 a tensile regime. We develop a conceptual model to describe how seepage may be controlled by an interplay  
20 between tectonic stresses and pore fluid pressure within shallow gas reservoirs across the passive margin off west-  
21 Svalbard. Glacio-isostatic flexural stresses may have influenced fluid dynamics along the Vestnesa Ridge in the  
22 past, explaining the presence of dormant pockmarks outside the ridge segment that is under a tensile regime at  
23 present and reconciling formerly suggested models of seepage periodicity linked to glacial cycles.

24

## 25 1. INTRODUCTION

26 Seafloor seepage is a wide-spread phenomenon which consists in the release of natural gases into the oceans.  
27 Hundreds of gigatonnes of carbon are stored as gas hydrates and shallow gas reservoirs in continental margins  
28 (e.g., Hunter et al., 2013). The release of these carbons over geological time is an important component of the  
29 global carbon cycle. Understanding and quantifying seepage has important implications for ocean acidification,  
30 deep-sea ecology and global climate. Periods of massive methane release from gas hydrate systems (e.g., Dickens,  
31 2011) or from large volcanic basins like that in the mid-Norwegian Margin (e.g., Svensen et al., 2004) have been  
32 linked to global warming events such as the Palaeocene-Eocene thermal maximum. We know that methane  
33 seepage has been occurring for millions of years, but we have a poor understanding of what forces it.

34

35 Present day seepage is identified as acoustic flares in the water column commonly originating at seafloor  
36 depressions, while authigenic carbonate mounds are used as indicators of longer-term seepage activity (e.g., Judd  
37 and Hovland, 2009). Seepage at the theoretical upstream termination of the gas hydrate stability zone (GHSZ) (i.e.,  
38 coinciding with the shelf edge) on different continental margins, has been explained by temperature driven gas-  
39 hydrate dissociation (e.g., Skarke et al., 2014; Westbrook et al., 2009). On formerly glaciated margins, active  
40 seepage is believed to be associated with pressure changes resulting from the retreat of the ice-sheet (e.g.,



41 Andreassen et al., 2017; Portnov et al., 2016). The effect of post-glaciation uplift on gas hydrate stability has been  
42 recently suggested as an alternative explanation for seepage localized at the shelf break offshore west-Svalbard  
43 (Wallmann et al., 2018)

44

45 Across the formerly glaciated west-Svalbard margin, active seepage extends beyond the shelf break and the region  
46 formerly covered by ice. As a matter of fact, active seepage sites have been identified from inside Isfjorden (Roy  
47 et al., 2014) to water depths of ~1200 m (Smith et al., 2014) where the Vestnesa Ridge hosts a perennially stable  
48 gas hydrate system beyond the ice-sheet grounding line. Seafloor pockmarks along the Vestnesa Ridge, first  
49 documented by Vogt (1994), exist along the entire ridge. However, acoustic flares have been observed to originate  
50 exclusively at large pockmarks located on the eastern part of the sedimentary ridge (Fig. 1,2). The presence of  
51 inactive pockmarks adjacent to a zone of active seepage along the Vestnesa Ridge, raises the question what stopped  
52 previously active seepage sites?

53

54 Plaza-Faverola et al., (2015) documented seismic differences in the orientation and type of faulting along the ridge  
55 and showed a link between the distribution of gas chimneys and faults. They suggested that tectonic stress  
56 variations may have a long-term effect on the spatial distribution of fault-related gas migration and seepage  
57 evolution. Here, we modelled the tectonic stress regime due to mid-ocean ridge spreading at Molloy and Knipovich  
58 ridges in Fram Strait, to test how spreading at these ridges influences the tectonic field along the Vestnesa Ridge.  
59 The tectonic model contributes with additional evidence of a correlation between regional stress regime and  
60 seepage patterns along the Vestnesa Ridge initially postulated based on seismic interpretation (Plaza-Faverola et  
61 al., 2015). Our study is in line with observations of earthquake-induced seafloor seepage (e.g., Geersen et al., 2016)  
62 and stress field variations (e.g., Plaza-Faverola et al., 2014) at accretionary margins suggesting that the effect of  
63 regional stresses on fluid dynamics in the near-surface has implications for seepage systems globally.

64

## 65 1. GEOLOGICAL SETTING OF THE VESTNESA RIDGE SEEPAGE SYSTEM

66 In Fram Strait, sedimentary basins are within tens of kilometres from ultra-slow spreading Arctic mid-ocean ridges  
67 (Fig. 1). The opening of the Fram Strait was initiated 33 Ma ago and evolved as a result of slow spreading of the  
68 Molloy and Knipovich Ridges (Engen et al., 2008). The circulation of deep water masses through Fram Strait  
69 started during the Miocene, ca. 17-10 Ma ago (Ehlers and Jokat, 2009; Jakobsson et al., 2007), establishing the  
70 environmental conditions for the evolution of bottom current-driven sedimentary drifts (Eiken and Hinz, 1993;  
71 Johnson et al., 2015). The NW-SE oriented Vestnesa sediment depocenter, extends for ca. 100 km off the west-  
72 Svalbard passive margin (Fig. 1b) and developed in the tectonically complex transition zone from oceanic to  
73 continental crust (Eiken and Hinz, 1993). In addition, the effect of ice-sheet dynamics on the west-Svalbard margin  
74 (Knies et al., 2009; Patton et al., 2016) has influenced the stratigraphy, and most likely the morphology, of the  
75 Vestnesa Ridge and adjacent sedimentary basins. The sedimentary succession along the Vestnesa Ridge is > 5 km  
76 thick in places and has been divided in three main stratigraphic units (Eiken and Hinz, 1993; Hustoft, 2009): the  
77 deepest sequence, YP1, consists of synrift and post-rift sediments deposited directly on oceanic crust; YP2 consists  
78 of contourites; and YP3, corresponding to the onset of Pleistocene glaciations (ca. 2.7 Ma ago) (Mattingsdal et al.,  
79 2014), is a mix of glaciomarine contourites and turbidites.

80



81 The gas hydrate system dynamics along the Vestnesa Ridge seems to be highly influenced by spatial variations in  
82 the geothermal gradient and the gas composition (Plaza-Faverola et al., 2017). Thermogenic gas is accumulating  
83 at the base of the GHSZ (Fig. 2) and part of this gas sustains present day seepage activity (Bünz et al., 2012; Plaza-  
84 Faverola et al., 2017). Seepage has been occurring at least since the onset of the Pleistocene glaciations c. 2.7 Ma  
85 ago (Plaza-Faverola et al., 2015). Many transient seepage events are suspected and one was dated to ca. 17.000  
86 years based on the presence of a ~1000 years old methane-dependent bivalve community possibly sustained by a  
87 gas pulse through a fault (Ambrose et al., 2015).

88

## 89 2. SEISMIC DATA

90 The description of faults and fluid flow related features along the Vestnesa Ridge is documented in Plaza-Faverola  
91 et al., 2015. The description is based on two-3D high resolution seismic data sets acquired on the western and the  
92 eastern Vestnesa Ridge segments respectively, and one 2D seismic line acquired along the entire Vestnesa Ridge  
93 extent (Fig. 2 this paper). These data have been previously used for the investigation of BSR dynamics (Plaza-  
94 Faverola et al., 2017) and documentation of gas chimneys and faults in the region (Petersen et al., 2010; Plaza-  
95 Faverola et al., 2015). The data were acquired on board R/V Helmer Hanssen using the 3D P-Cable system (Planke  
96 et al., 2009). Final lateral resolution of the 3D data sets is given by a bin size of 6.25x6.25 m<sup>2</sup> and the vertical  
97 resolution is > 3 m with a dominant frequency of 130 Hz. Details about acquisition and processing can be found  
98 in Petersen et al., 2010 and Plaza-Faverola et al., 2015. For the 2D survey the dominant frequency was ~80 Hz  
99 resulting in a vertical resolution > 4.5 m (assumed as  $\lambda/4$  with an acoustic velocity in water of 1469 m/s given by  
100 CTD data; Plaza-Faverola et al., 2017).

101

## 102 3. THE MODELING APPROACH

103 Tectonic processes at plate margins have a major influence on regional stress patterns (Heidbach et al., 2010).  
104 Given the proximity to the Molloy and Knipovich Ridges, it is likely that ridge push has a major control on the  
105 regional, tectonic stress field on Vestnesa Ridge. Other stress sources of importance in the region are gravitational  
106 stresses due to bathymetry/topography and subsurface density contrasts and flexural stresses due to sediment  
107 erosion and deposition. During the Quaternary, the west-Svalbard margin was furthermore affected by glacially  
108 induced flexural stresses due to the glaciations. Here, we focus on the tectonic stress due to ridge push. We use the  
109 approach by Keiding et al. (2009) based on the analytical solutions derived by Okada (1985), to model the plate  
110 motion and tectonic stress field due to spreading along the Molloy and Knipovich Ridges. Because the model only  
111 incorporates plate spreading, it is likely that the actual stress field on the west-Svalbard margin differs to some  
112 extent from the stress field predicted by our model. However, by excluding all other sources of stress, we are able  
113 to investigate the influence of tectonic stress exclusively.

114 The Okada model and our derivation of the stress field from it is described in more detail in appendix A. The  
115 Molloy and Knipovich Ridges are modelled as rectangular planes with opening and transform motion in a flat  
116 earth model with elastic, homogeneous, isotropic rheology. Each rectangular plane is defined by ten model  
117 parameters used to approximate the location, geometry and deformation of the spreading ridges (Okada, 1985; see  
118 supplement Table 1). The locations of the two spreading ridges were constrained from bathymetry maps (Fig. 3).  
119 The two spreading ridges are assumed to have continuous deformation below the brittle-ductile transition, with a  
120 half spreading rate of 7 mm/yr and a spreading direction of N125°E, according to recent plate motion models



121 (DeMets et al., 2010). Because the spreading direction is not perpendicular to the trends of the spreading ridges,  
122 this results in both opening and right-lateral motion; that is, oblique spreading on the Molloy and Knipovich  
123 Ridges. The Molloy Transform Fault, which connects the two spreading ridges, trends N133°E, thus a spreading  
124 direction of N125°E implies extension across the transform zone. We use a depth of 10 km for the brittle-ductile  
125 transition and 900 km for the lower boundary of the deforming planes, to avoid boundary effects. For the elastic  
126 rheology, we assume typical crustal values of Poisson's ratio = 0.25 and shear modulus = 30 GPa (Turcotte and  
127 Schubert, 2002).

128

129 We focus on the stress field in the upper part of the crust (where the GHSZ is) and characterise the stress regime  
130 based on the relative magnitudes of the horizontal and vertical stresses. We refer to the stresses as  $\sigma_v$  (vertical  
131 stress),  $\sigma_H$  (maximum horizontal stress) and  $\sigma_h$  (minimum horizontal stress), where compressive stress is positive  
132 (Zoback and Zoback, 2002). A tensile stress regime ( $\sigma_v > \sigma_H > \sigma_h$ ) favours the opening of steep faults that can  
133 provide pathways for fluids. Compressive ( $\sigma_H > \sigma_h > \sigma_v$ ) and strike-slip ( $\sigma_H > \sigma_v > \sigma_h$ ) regimes do not favour such  
134 opening (e.g., Graults and Baleix, 1994).

135

136 The model predicts zones of tensile stress near the spreading ridges, and strike-slip at larger distance from the  
137 ridges. Despite the simplicity of the model assumptions, the agreement between predicted stress regime and  
138 observed earthquake focal mechanisms is reassuring, with normal faulting mechanisms along the ridges and strike-  
139 slip mechanisms dominating everywhere else, particularly along the Spitsbergen and Molloy Transform Faults  
140 (Fig. 3).

141

142 An unexpected pattern arises near the Vestnesa Ridge due to the interference of the stress from the two spreading  
143 ridges. A zone of tensile stress extends northward from the Knipovich Ridge, encompassing the eastern part of the  
144 Vestnesa Ridge. The western Vestnesa Ridge, on the other hand, lies entirely in a zone of strike-slip stress (Fig.  
145 3). Sensitivity tests for realistic variations in 1) mid-oceanic spreading, 2) depth of the brittle-ductile transition,  
146 and 3) elastic moduli, show that the tensile stress zone covering the eastern Vestnesa Ridge is a robust feature of  
147 the model, that is, variations in the parameters result in a change of the extent and shape of the tensile zone but the  
148 zone remains in place (Supplementary material).

149

#### 150 4. CORRELATION BETWEEN MODELLED TECTONIC STRESS REGIME, FAULTING AND 151 SEEPAGE

152 The zone of tensile stress on the eastern Vestnesa Ridge coincides with a zone of faulting and restricted seepage  
153 at the crest of the Vestnesa Ridge (Fig. 2, 3). The match between the extend of the modelled tensile zone and the  
154 active pockmarks is not exact; active pockmarks exist a few kilometres westward from the termination of the  
155 tensile zone (Fig. 3). However, the agreement is striking from a regional point of view, considering the uncertainty  
156 of the model as illustrated by the sensitivity tests (Supplementary material). In the predicted tensile zone towards  
157 the east of the Vestnesa Ridge, the sub-seabed faults are NW-SE oriented, near vertical and have a gentle normal  
158 throw (< 10 m). They are spatially linked to gas chimneys and active seepage (Bünz et al., 2012; Plaza-Faverola  
159 et al., 2015). Some of the faults show thicker sediment thicknesses at the hanging wall, allowing identification of  
160 discrete periods of faulting (Plaza-Faverola et al., 2015). The character of the faults changes towards the western



161 Vestnesa Ridge and the predicted strike-slip regime. The density of faulting and seismic definition decreases  
162 westward (Fig. 2, 4). In this part of the ridge gas chimneys are narrower, stacked more vertically than active  
163 chimneys towards the east and it is possible to recognise more faults reaching the present-day seafloor (Plaza-  
164 Faverola et al., 2015).

165

166 A cluster of larger scale N-S to NNW-SSE trending extensional faults outcrop at the southern slope of the Vestnesa  
167 Ridge, also within the zone of predicted tensile stress (Fig. 1, 3). In agreement with our models, these extensional  
168 faults have been suggested to indicate the northward propagation of the Knipovich Ridge rift system (Crane et al.,  
169 2001; Vanneste et al., 2005). However, it is likely that faulting along this steep slope of the Vestnesa Ridge (Fig.  
170 1) was partially induced by gravitational stress.

171

172 The striking correlation between predicted tectonic stress regime, faulting structures and current seepage does, in  
173 fact, suggest that tectonic stress has potentially a major influence on the near-surface sedimentary deformation.  
174 Hereafter, we discuss the implications of the interaction between tectonic stresses and pore-fluid pressure for the  
175 evolution of gas seepage along the Vestnesa Ridge.

176

##### 177 5. SEEPAGE COUPLED TO STRESS CYCLING

178 Based on the correlation between tectonic stress regimes and seepage patterns, we postulate that current seepage  
179 at the eastern Vestnesa Ridge segment is favoured by the opening of pre-existing faults in a tensile stress regime  
180 (Fig. 2b). Depending on the tectonic regime, permeability through faults and fractures may be enhanced or  
181 inhibited (e.g., Hillis, 2001; Sibson, 1994). Thus, spatial and temporal variations in the tectonic stress regime may  
182 control the transient release of gas from the seafloor over geological time as documented for example for CO<sub>2</sub>  
183 analogues in the Colorado Plateau (e.g., Jung et al., 2014). We conjecture that seepage along the Vestnesa Ridge  
184 has been driven by cycles of increased secondary permeability via the formation of tension fractures near faults or  
185 brecciation of fault zones. Formation of tension fractures is facilitated if the minimum horizontal stress is smaller  
186 than the pore-fluid pressure ( $p_f$ ), that is, the minimum effective stress is negative ( $\sigma_h' = \sigma_h - p_f < 0$ ) (e.g., Grauls  
187 and Baleix, 1994). A negative minimum effective stress and subsequent increase in secondary permeability in a  
188 tensile stress regime can be achieved particularly easy in the near-surface. Continued flow through opened faults  
189 and fractures may lead to brecciation and development of seismic chimneys (Fig. 2b) (Sibson, 1994).

190

191 The steep NW-SE oriented faults mapped along the Vestnesa Ridge may have formed in a strike-slip regime but  
192 become permeable for gas accumulated beneath the GHSZ in periods of tensile stress. We suggest that the eastern  
193 Vestnesa Ridge segment is currently in a phase of stress relaxation where  $\sigma_h$  is close to zero and  $\sigma_h'$  is negative,  
194 due to high pore-fluid pressure at the base of the GHSZ (i.e., the shallowest reservoir holding gas from escaping  
195 to the seafloor). A high pressure at the base of the GHSZ in this part of the ridge is explained by a constant input  
196 of thermogenic gas from an Eocene reservoir since at least ca. 2 Ma ago (Knies et al., in press). Along the western  
197 Vestnesa Ridge, on the other hand, the fluid pressure at the base of the GHSZ would not be high enough to  
198 overcome the minimum horizontal stress and seepage is thus not promoted at present (Fig. 2a).

199



200 While the tectonic stress is constant over short geological time spans, the chimney development and seafloor  
201 seepage has been a transient process because of slight variations in pore-fluid pressure or the influence of other  
202 stress generating mechanisms that bring the system out of equilibrium. Geophysical and paleontological data  
203 indicate that there was once seepage and chimney development on the western Vestnesa Ridge segment (e.g.,  
204 Consolaro et al., 2015; Plaza-Faverola et al., 2015). Past seepage through faults may have been repeatedly incited  
205 by glacially induced horizontal stresses during Quaternary glaciations (Fig. 4). During glacial periods, the load of  
206 the ice forces the lithosphere down and creates an isostatic forebulge along the periphery of the ice, generating  
207 considerable flexural stresses in the upper part of the lithosphere (Lund and Schmidt, 2011). The lateral expansion  
208 of grounded ice in the western Barents Sea region is limited by the continental shelf break, and the Vestnesa Ridge  
209 was likely affected by tensional flexural stresses in the forebulge around the time of glacial maximums (Patton et  
210 al., 2016). We consider it likely that the repeated waxing and waning of the ice sheet caused a cyclic modulation  
211 of the stress field and influenced the dynamics of gas accumulations along the Vestnesa Ridge in the past; thus  
212 explaining the correlation between past seepage and glaciation events observed in other continental margins e.g.,  
213 for chimneys off the mid-Norwegian margin (Plaza-Faverola et al., 2011), the Gulf of Lion (Riboulot et al., 2014),  
214 but also along the Vestnesa Ridge (Plaza-Faverola et al., 2015).

215

216 A long-term variation in tectonic stress on the Vestnesa Ridge is caused by its location on a constantly growing  
217 plate. As the oceanic plate grows, Vestnesa Ridge moves eastward with respect to the Molloy and Knipovich  
218 Ridges, causing a westward shift in the regional stress field on Vestnesa Ridge (Fig. 5). In the future, the eastern  
219 Vestnesa Ridge may temporarily move out of the tensile zone, while the western Vestnesa Ridge moves into it  
220 (Fig. 5). This suggests that active seepage may reappear at pockmarks to the west of the currently active seepage  
221 zone.

222

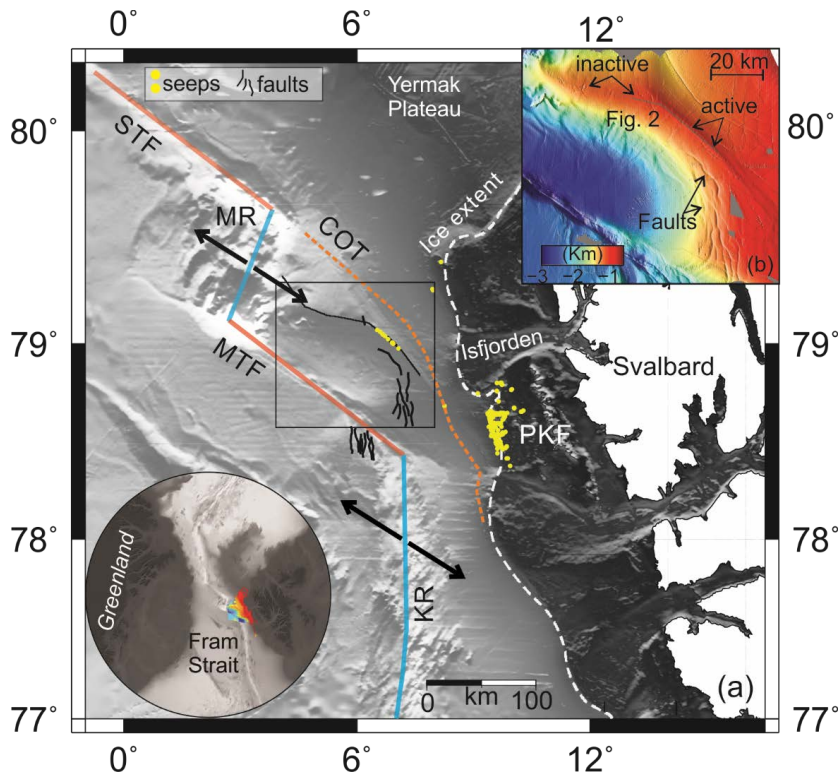
## 223 6- CONCLUSIONS

224 The results of modelling the stress regime generated exclusively by mid-ocean ridge spreading in Fram Strait  
225 support seismic evidence of the correlation between faulting and seepage distribution along the Vestnesa  
226 sedimentary ridge, offshore the west Svalbard margin. Tectonic stresses due to oblique spreading along the Molloy  
227 and the Knipovich ridges influences the present day stress field across the west-Svalbard passive margin. A  
228 correlation between a tensile stress regimes and seepage activity suggests that episodic seepage through gas  
229 chimneys has been controlled by an interplay between varying minimum horizontal stresses and pore fluid pressure  
230 at the free gas zone beneath the hydrate reservoir. Present-day seepage is facilitated by opening of faults and  
231 fractures in a tensile stress regime, where pore fluid pressure overcome the minimum horizontal stress. Pockmarks  
232 that are inactive at present under a strike-slip regime, but were active multiple times in the past, may have been  
233 activated by additional tensile stresses (e.g., from glacial related lithospheric adjustments). Future reactivation of  
234 currently dormant pockmarks is likely following the gradual westward propagation of the tensile stress zone on  
235 the Vestnesa Ridge.

236

## 237 Figures





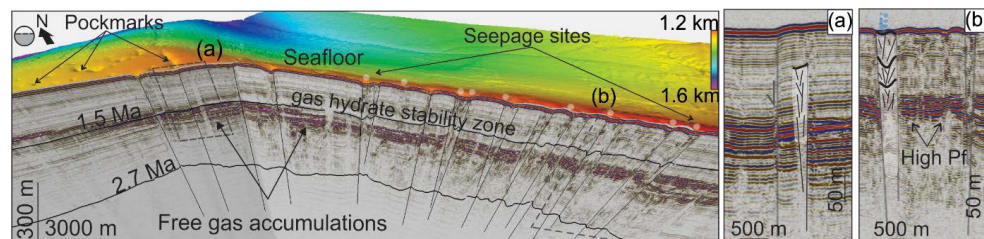
238

239 **Figure 1:** (a) International Bathymetry Chart of the Arctic Ocean (IBCAO) showing the geometry of mid-ocean  
 240 ridges offshore the west-Svalbard margin; (b) High resolution bathymetry along the Vestnesa Ridge (UiT, R/V  
 241 HH multi-beam system). Seafloor pockmarks are observed along the entire ridge but active seep sites are restricted  
 242 to its eastern segment; PKF=Prins Karl Foreland; STF=Spitsbergen Transform Fault; MR=Molloy Ridge;  
 243 MTF=Molloy Transform Fault; KR=Knipovich Ridge; COT=Continental-Oceanic Transition (Engen et al., 2008);  
 244 Ice-Sheet Extent (Patton et al., 2016).

245

246

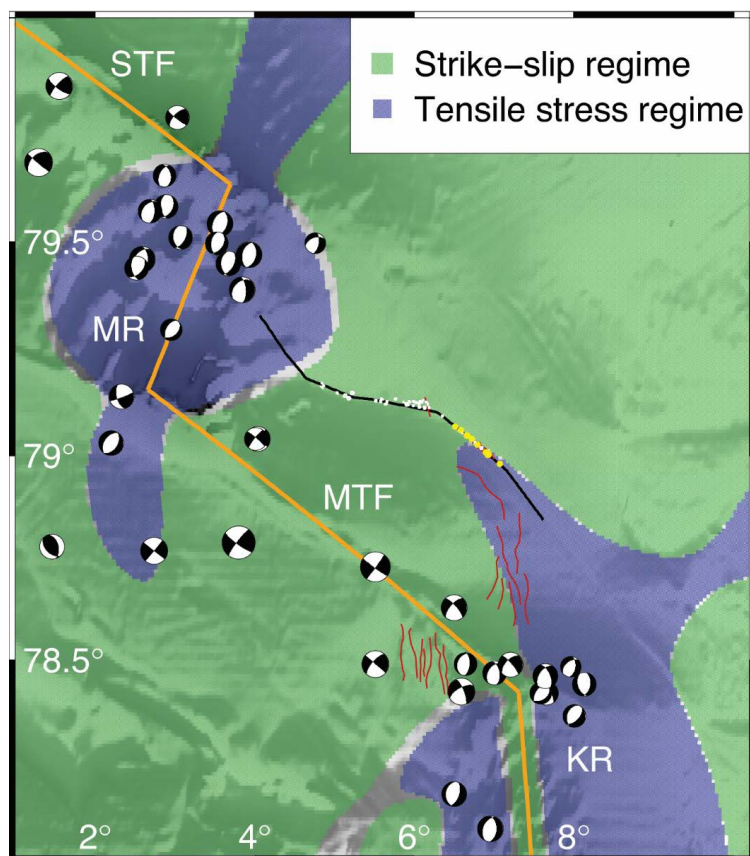
247



248

249 **Figure 2:** Integrated seismic and bathymetry image of the gas hydrate system along the Vestnesa Ridge. (a)  
 250 Outcropping fault located at the transition from the active to the currently inactive pockmark region; (b) Gas  
 251 chimneys with active seepage and inferred high pore-fluid pressure (Pf) zone.

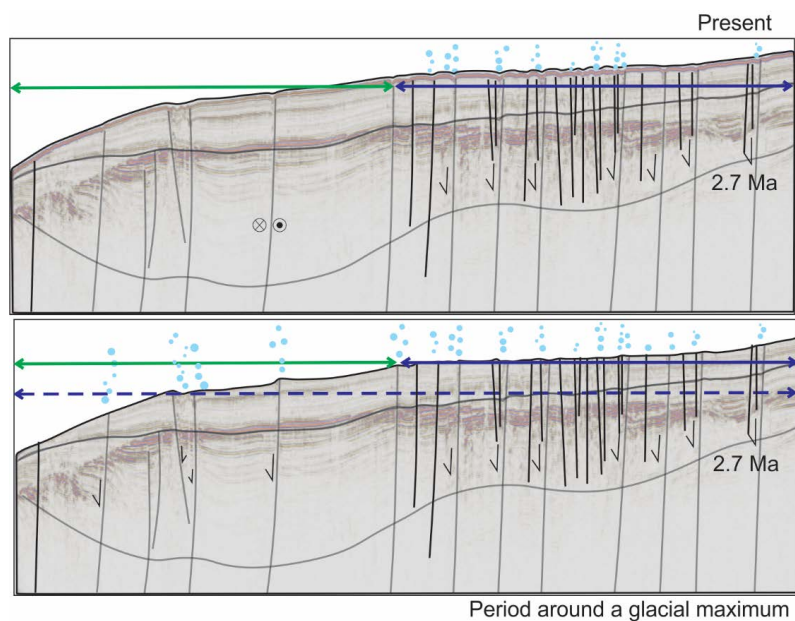
252



253

254 **Figure 3:** Modelled upper crustal tectonic stress field (blue – tensile and green - strike-slip regime), due to oblique  
255 spreading at Molloy Ridge (MR) and Knipovich Ridge (KR). The seismic line is projected as reference for the  
256 crest of the Vestnesa Ridge. Red lines are faults, yellow dots seeps and white circles inactive pockmarks. The focal  
257 mechanisms are from the ISC Online Bulletin (<http://www.isc.ac.uk>).





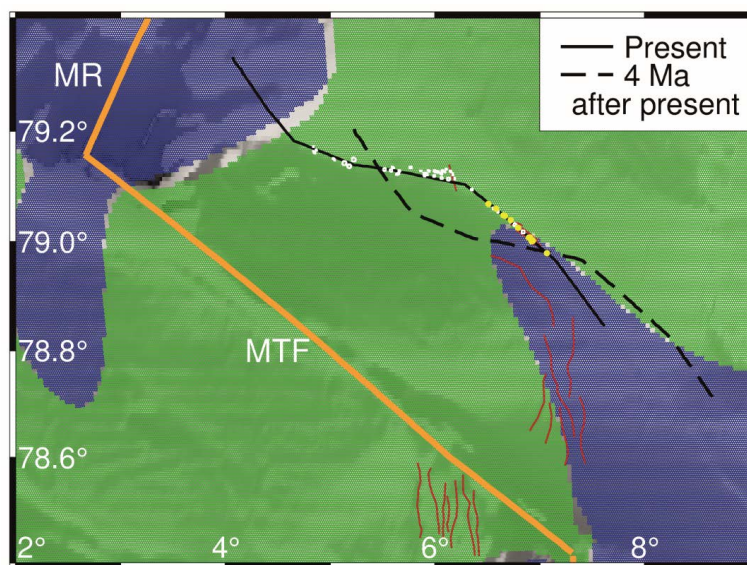
258

259 **Figure 4:** Conceptual model of the evolution of seepage coupled to faulting and spatial variations in the stress  
260 regime (tensile=blue; strike-slip=green) along the Vestnesa Ridge, offshore the west-Svalbard margin. At present  
261 day, tensile stress from mid-ocean ridge spreading (blue solid line) favours seepage exclusively on the eastern  
262 segment of the Vestnesa Ridge. Seepage on the western Vestnesa Ridge and other regions may have been induced  
263 repeatedly since the onset of glaciations 2.7 Ma ago (Mattingsdal et al., 2014), due to tensile flexural stresses in  
264 the isostatic forebulge around the time of glacial maximums.

265

266

267



268

269 **Figure 5:** Stress field in figure 3 showing the location of the Vestnesa Ridge at present and 4 Ma after present  
270 time, assuming a constant spreading velocity of 7 mm/yr in the direction N125°E. The black polygon corresponds  
271 to the seismic line in Plaza-Faverola et al., 2017 and partly shown in figure 2. It is presented as reference for the  
272 crest of the eastern and western Vestnesa Ridge segments

273

## 274 **Appendix A**

### 275 **Model description**

276

277 We use the analytical formulations of Okada (1985) for a finite rectangular dislocation source in elastic  
278 homogeneous isotropic half-space (Fig. A.1). The dislocation source can be used to approximate deformation  
279 along planar surfaces, such as volcanic dykes (e.g. Wright et al., 2006), sills (e.g. Pedersen and Sigmundsson,  
280 2004), faults (e.g. Massonet et al, 1993) and spreading ridges (e.g. Keiding et al., 2009). More than one dislocations  
281 can be combined to obtain more complex geometry of the source or varying deformation along a planar source.  
282 The deformation of the source can be defined as either lateral shear (strike-slip for faults), vertical shear (dip-slip  
283 at faults) or tensile opening.

284

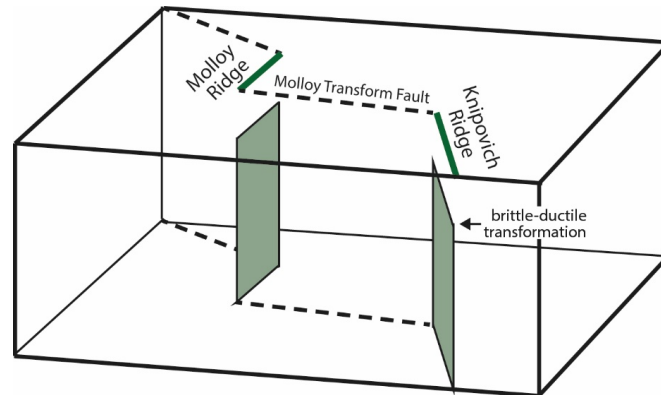
285 The Okada model assumes flat Earth without inhomogeneities. While the flat-earth assumption is usually adequate  
286 for regional studies (e.g. Wolf, 1984), the lateral inhomogeneities can sometimes cause considerable effect on the  
287 deformation field (e.g. Okada, 1985). However, the dislocation model is useful as a first approximation to the  
288 problem.

289

290 At mid-ocean ridges, deformation is driven by the continuous spreading caused primarily by gravitational stress  
291 due to the elevation of the ridges, but also basal drag and possibly slab pull. Deformation occurs continuously in  
292 the ductile part of the crust. Meanwhile, elastic strain builds in the upper, brittle part of the crust. To model this



293 setting, the upper boundary of the dislocation source must be located at the depth of the brittle-ductile transition  
 294 zone. The lower boundary of the source is set to some arbitrary large depth to avoid boundary effects.  
 295



296  
 297 **Fig A.1** Extract of model showing the location of the dislocation sources (light green) for Molloy and  
 298 **Knipovich ridges**. Note that the model is an infinite half-space, i.e. it has no lateral or lower boundary.  
 299

300 The Okada model provides the displacements  $u_x$ ,  $u_y$ ,  $u_z$  (or velocities if deformation is time-dependent) at defined  
 301 grid points at the surface and subsurface. It also provides strain (or strain rates) defined as:

$$302 \quad \varepsilon_{ij} = \frac{1}{2}(u_{i,j} + u_{j,i})$$

303 The stress field can then be calculated from the predicted strain rates. In homogeneous isotropic media, stress is  
 304 related to strain as:

$$305 \quad \sigma_{ij} = \lambda \delta_{ij} \varepsilon_{kk} + 2\mu \varepsilon_{ij}$$

306 where  $\delta_{ij}$  is the Kronecker delta,  $\lambda$  is Lamé's first parameter, and  $\mu$  is the shear modulus. Lamé's first parameter  
 307 does not have a physical meaning but is related to the shear modulus and Poisson's ratio ( $\nu$ ) as  $\lambda = \frac{2\mu\nu}{1-2\nu}$ .

308 The absolute values of stress are in general difficult to model (e.g. Hergert and Heidbach, 2011), and not possible  
 309 with our analytical model. However, the model provides us with the orientations and relative magnitude of the  
 310 stresses. That is, we know the relative magnitudes of the vertical stress ( $\sigma_v$ ), maximum horizontal stress ( $\sigma_H$ ) and  
 311 minimum horizontal stress ( $\sigma_h$ ). From this, the stress regime can be defined as either tensile ( $\sigma_v > \sigma_H > \sigma_h$ ), strike-  
 312 slip ( $\sigma_H > \sigma_v > \sigma_h$ ) or compressive ( $\sigma_H > \sigma_h > \sigma_v$ ).

313

### 314 **Author contribution**

315 Andreia Plaza-Faverola conceived the paper idea. She is responsible for seismic data processing and interpretation.  
 316 Marie Keiding did the tectonic modelling. The paper is the result of integrated work between both.

317

### 318 **ACKNOWLEDGEMENTS**

319 This research is part of the Centre for Arctic Gas Hydrate, Environment and Climate (CAGE) supported by the  
 320 Research Council of Norway through its Centres of Excellence funding scheme grant No. 223259. Marie Keiding  
 321 is supported by the NEONOR2 project at the Geological Survey of Norway. Seismic data is archived at CAGE –



322 Centre for Arctic Gas Hydrate, Environment and Climate, Tromsø, Norway and can be made available by  
323 contacting APF. Modelled stresses can be made available by contacting MK.

324

325 **References:**

326 Ambrose, W.G., Panieri, G., Schneider, A., Plaza-Faverola, A., Carroll, M.L., Åström, E.K., Locke, W.L.,  
327 Carroll, J., 2015. Bivalve shell horizons in seafloor pockmarks of the last glacial-interglacial transition: a  
328 thousand years of methane emissions in the Arctic Ocean. *Geochemistry, Geophysics, Geosystems* 16, 4108-  
329 4129.

330

331 Andreassen, K., Hubbard, A., Winsborrow, M., Patton, H., Vadakkepuliambatta, S., Plaza-Faverola, A.,  
332 Gudlaugsson, E., Serov, P., Deryabin, A., Mattingsdal, R., 2017. Massive blow-out craters formed by hydrate-  
333 controlled methane expulsion from the Arctic seafloor. *Science* 356, 948-953.

334

335 Argus, D.F., Gordon, R.G., Heflin, M.B., Ma, C., Eanes, R.J., Willis, P., Peltier, W.R., Owen, S.E., 2010. The  
336 angular velocities of the plates and the velocity of Earth's centre from space geodesy. *Geophysical Journal*  
337 *International* 180, 913-960.

338

339 Bünz, S., Polyanov, S., Vadakkepuliambatta, S., Consolaro, C., Mienert, J., 2012. Active gas venting through  
340 hydrate-bearing sediments on the Vestnesa Ridge, offshore W-Svalbard. *Marine geology*.

341 Consolaro, C., Rasmussen, T., Panieri, G., Mienert, J., Bünz, S., Szybor, K., 2015. Carbon isotope ( $\delta^{13}\text{C}$ )  
342 excursions suggest times of major methane release during the last 14 kyr in Fram Strait, the deep-water gateway  
343 to the Arctic. *Climate of the Past* 11, 669-685.

344

345 Crane, K., Doss, H., Vogt, P., Sundvor, E., Cherkashov, G., Poroshina, I., Joseph, D., 2001. The role of the  
346 Spitsbergen shear zone in determining morphology, segmentation and evolution of the Knipovich Ridge. *Marine*  
347 *geophysical researches* 22, 153-205.

348

349 DeMets, C., Gordon, R.G., Argus, D.F., 2010. Geologically current plate motions. *Geophysical Journal*  
350 *International* 181, 1-80.

351

352 Dickens, G.R., 2011. Down the rabbit hole: Toward appropriate discussion of methane release from gas hydrate  
353 systems during the Paleocene-Eocene thermal maximum and other past hyperthermal events. *Climate of the Past*  
354 7, 831-846.

355

356 Ehlers, B.-M., Jokat, W., 2009. Subsidence and crustal roughness of ultra-slow spreading ridges in the northern  
357 North Atlantic and the Arctic Ocean. *Geophysical Journal International* 177, 451-462.

358

359 Eiken, O., Hinz, K., 1993. Contourites in the Fram Strait. *Sedimentary Geology* 82, 15-32.

360

361 Engen, Ø., Faleide, J.I., Dyreng, T.K., 2008. Opening of the Fram Strait gateway: A review of plate tectonic  
362 constraints. *Tectonophysics* 450, 51-69.

363

364 Geersen, J., Scholz, F., Linke, P., Schmidt, M., Lange, D., Behrmann, J.H., Völker, D., Hensen, C., 2016. Fault  
365 zone controlled seafloor methane seepage in the rupture area of the 2010 Maule Earthquake, Central Chile.  
366 *Geochemistry, Geophysics, Geosystems* 17, 4802-4813.

367

368 Grauls, D., Baleix, J., 1994. Role of overpressures and in situ stresses in fault-controlled hydrocarbon migration:  
369 A case study. *Marine and Petroleum Geology* 11, 734-742.

370

371 Heidbach, O., Tingay, M., Barth, A., Reinecker, J., Kurfeß, D., Müller, B., 2010. Global crustal stress pattern  
372 based on the World Stress Map database release 2008. *Tectonophysics* 482, 3-15.

373

374 Hergert, T., and Heidbach, O., 2011. Geomechanical model of the Marmara Sea region – II. 3-D contemporary  
375 background stress field. *Geophys. J. Int.* 185, 1090-1102, doi: 10.1111/j.1365-246X.2011.04992.x.

376

377 Hillis, R.R., 2001. Coupled changes in pore pressure and stress in oil fields and sedimentary basins. *Petroleum*  
378 *Geoscience* 7, 419-425.

379



- 380 Hunter, S., Goldobin, D., Haywood, A., Ridgwell, A., Rees, J., 2013. Sensitivity of the global submarine hydrate  
381 inventory to scenarios of future climate change. *Earth and Planetary Science Letters* 367, 105-115.  
382
- 383 Hustoft, S., Bunz, S., Mienert, J., Chand, S., 2009. Gas hydrate reservoir and active methane-venting province in  
384 sediments on < 20 Ma young oceanic crust in the Fram Strait, offshore NW-Svalbard. *Earth and Planetary  
385 Science Letters* 284, 12-24.  
386
- 387 Jakobsson, M., Backman, J., Rudels, B., Nycander, J., Frank, M., Mayer, L., Jokat, W., Sangiorgi, F., O'Regan,  
388 M., Brinkhuis, H., 2007. The early Miocene onset of a ventilated circulation regime in the Arctic Ocean. *Nature*  
389 447, 986-990.  
390
- 391 Johnson, J.E., Mienert, J., Plaza-Faverola, A., Vadakkepulyambatta, S., Knies, J., Bünz, S., Andreassen, K.,  
392 Ferré, B., 2015. Abiotic methane from ultraslow-spreading ridges can charge Arctic gas hydrates. *Geology*,  
393 G36440. 36441.
- 394 Judd, A., Hovland, M., 2009. Seabed fluid flow: the impact on geology, biology and the marine environment.  
395 Cambridge University Press.  
396
- 397 Jung, N.-H., Han, W.S., Watson, Z., Graham, J.P., Kim, K.-Y., 2014. Fault-controlled CO<sub>2</sub> leakage from natural  
398 reservoirs in the Colorado Plateau, East-Central Utah. *Earth and Planetary Science Letters* 403, 358-367.  
399
- 400 Keiding, M., Lund, B., Árnadóttir, T., 2009. Earthquakes, stress, and strain along an obliquely divergent plate  
401 boundary: Reykjanes Peninsula, southwest Iceland. *Journal of Geophysical Research: Solid Earth* 114.  
402
- 403 Knies, J., Matthiessen, J., Vogt, C., Laberg, J.S., Hjelstuen, B.O., Smelror, M., Larsen, E., Andreassen, K.,  
404 Eidvin, T., Vorren, T.O., 2009. The Plio-Pleistocene glaciation of the Barents Sea–Svalbard region: a new model  
405 based on revised chronostratigraphy. *Quaternary Science Reviews* 28, 812-829.  
406
- 407 Lund, B., Schmidt, P., 2011. Stress evolution and fault stability at Olkiluoto during the Weichselian glaciation.  
408 Posiva Oy.  
409
- 410 Massonet, D., Rossi, M., Carmona, C., Adragna, F., Peltzer, G., Feigl, K., and Rabaute, T., 1993. The  
411 displacement field of the Landers earthquake mapped by radar interferometry. *Nature* 364, 138-142.
- 412 Mattingsdal, R., Knies, J., Andreassen, K., Fabian, K., Husum, K., Grøsfjeld, K., De Schepper, S., 2014. A new  
413 6 Myr stratigraphic framework for the Atlantic–Arctic Gateway. *Quaternary Science Reviews* 92, 170-178.
- 414 Okada, Y., 1985. Surface deformation due to shear and tensile faults in a half-space. *Bulletin of the  
415 seismological society of America* 75, 1135-1154.  
416
- 417 Patton, H., Hubbard, A., Andreassen, K., Winsborrow, M., Stroeven, A.P., 2016. The build-up, configuration,  
418 and dynamical sensitivity of the Eurasian ice-sheet complex to Late Weichselian climatic and oceanic forcing.  
419 *Quaternary Science Reviews* 153, 97-121.  
420
- 421 Pedersen, R., and Sigmundsson, F., 2004. InSAR based sill model links spatially offset areas of deformation and  
422 seismicity for the 1994 unrest at Eyjafjallajökull volcano, Iceland. *Solid Earth* 31, doi: 10.1029/2004GL020368.
- 423 Petersen, C.J., Bünz, S., Hustoft, S., Mienert, J., Klaeschen, D., 2010. High-resolution P-Cable 3D seismic  
424 imaging of gas chimney structures in gas hydrated sediments of an Arctic sediment drift. *Marine and Petroleum  
425 Geology* doi: 10.1016/j.marpetgeo.2010.06.006, 1-14.
- 426 Planke, S., Eriksen, F.N., Berndt, C., Mienert, J., Masson, D., 2009. P-Cable high-resolution seismic.  
427 *Oceanography* 22, 85.Plaza-Faverola, A., Bünz, S., Mienert, J., 2011. Repeated fluid expulsion through sub-  
428 seabed chimneys offshore Norway in response to glacial cycles. *Earth and Planetary Science Letters* 305, 297-  
429 308.
- 430 Plaza-Faverola, A., Bünz, S., Johnson, J.E., Chand, S., Knies, J., Mienert, J., Franek, P., 2015. Role of tectonic  
431 stress in seepage evolution along the gas hydrate-charged Vestnesa Ridge, Fram Strait. *Geophysical Research  
432 Letters* 42, 733-742.
- 433 Plaza-Faverola, A., Pecher, I., Crutchley, G., Barnes, P.M., Bünz, S., Golding, T., Klaeschen, D., Papenberg, C.,  
434 Bialas, J., 2014. Submarine gas seepage in a mixed contractional and shear deformation regime: Cases from the  
435 Hikurangi oblique-subduction margin. *Geochemistry, Geophysics, Geosystems* 15, 416-433.



- 436 Plaza-Faverola, A., Vadakkepuliambatta, S., Hong, W.L., Mienert, J., Bünz, S., Chand, S., Greinert, J., 2017.  
437 Bottom-simulating reflector dynamics at Arctic thermogenic gas provinces: an example from Vestnesa Ridge,  
438 offshore west-Svalbard. *Journal of Geophysical Research: Solid Earth*.
- 439 Portnov, A., Vadakkepuliambatta, S., Mienert, J., Hubbard, A., 2016. Ice-sheet-driven methane storage and  
440 release in the Arctic. *Nature communications* 7. Riboulot, V., Thomas, Y., Berné, S., Jouet, G., Cattaneo, A.,  
441 2014. Control of Quaternary sea-level changes on gas seeps. *Geophysical Research Letters* 41, 4970-4977.
- 442 Roy, S., Senger, K., Braathen, A., Noormets, R., Hovland, M., Olausson, S., 2014. Fluid migration pathways to  
443 seafloor seepage in inner Isfjorden and Adventfjorden, Svalbard. *Geological controls on fluid flow and seepage*  
444 in western Svalbard fjords, Norway. An integrated marine acoustic study. Sibson, R.H., 1994. Crustal stress,  
445 faulting and fluid flow. *Geological Society, London, Special Publications* 78, 69-84.
- 446 Skarke, A., Ruppel, C., Kodis, M., Brothers, D., Lobecker, E., 2014. Widespread methane leakage from the sea  
447 floor on the northern US Atlantic margin. *Nature Geoscience* 7, 657-661. Smith, A.J., Mienert, J., Bünz, S.,  
448 Greinert, J., 2014. Thermogenic methane injection via bubble transport into the upper Arctic Ocean from the  
449 hydrate-charged Vestnesa Ridge, Svalbard. *Geochemistry, Geophysics, Geosystems*.
- 450 Svensen, H., Planke, S., Malthe-Sørenssen, A., Jamtveit, B., Myklebust, R., Eidem, T.R., Rey, S.S., 2004.  
451 Release of methane from a volcanic basin as a mechanism for initial Eocene global warming. *Nature* 429, 542-  
452 545.
- 453 Turcotte, D.L., Schubert, G., 2002. *Geodynamics*. Cambridge University Press.
- 454 Vanneste, M., Guidard, S., Mienert, J., 2005. Arctic gas hydrate provinces along the western Svalbard  
455 continental margin. *Norwegian Petroleum Society Special Publications* 12, 271-284.
- 456 Vogt, P.R., Crane, K., Sundvor, E., Max, M.D., Pfirman, S.L., 1994. Methane-generated (?) pockmarks on  
457 young, thickly sedimented oceanic crust in the Arctic: Vestnesa ridge, Fram strait. *Geology* 22, 255-258.
- 458 Wallmann, K., Riedel, M., Hong, W., Patton, H., Hubbard, A., Pape, T., Hsu, C., Schmidt, C., Johnson, J.,  
459 Torres, M., 2018. Gas hydrate dissociation off Svalbard induced by isostatic rebound rather than global  
460 warming. *Nature communications* 9, 83.
- 461 Westbrook, G.K., Thatcher, K.E., Rohling, E.J., Piotrowski, A.M., Palike, H., Osborne, A.H., Nisbet, E.G.,  
462 Minshull, T.A., Lanoiselle, M., James, R.H., Hühnerbach, V., Green, D., Fisher, R.E., Crocker, A.J., Chabert, A.,  
463 Bolton, C., Beszczynska-Moller, A., Berndt, C., Aquilina, A., 2009. Escape of methane gas from the seabed  
464 along the West Spitsbergen continental margin. *Geophysical Research Letters* 36, 5.  
465
- 466 Wolf, D., 1984. The relaxation of spherical and flat Maxwell Earth models and the effects due to the presence of  
467 the lithosphere. *Journal of Geophysics – Zeitschrift für Geophysik* 56, 24-33.
- 468 Wright, T. J., Ebinger, C., Biggs, J., Ayele, A., Yirgu, G., Keir, D., and Stork, A., 2006. Magma-maintained rift  
469 segmentation at continental rapture in the 2005 Afar dyking episode. *Nature* 442, 291-294,  
470 doi:10.1038/nature04978.
- 471 Zoback, M.D., Zoback, M.L., 2002. 34 State of stress in the Earth's lithosphere. *International Geophysics* 81,  
472 559-XII.